Observation of Hourglass Nodal Lines in Photonics

Lingbo Xia, Qinghua Guo, Biao Yang, Jiaguang Han, Chao-Xing Liu, Weili Zhang, and Shuang Zhang

Phys. Rev. Lett. **122**, 103903 — Published 15 March 2019

DOI: 10.1103/PhysRevLett.122.103903

Observation of Hourglass Nodal Lines in Photonics

Lingbo Xia[1, 2*], Qinghua Guo[1*], Biao Yang[1,3*], Jiaguang Han[2,†], Chao-Xing Liu[4,††],

Weili Zhang[2,5], Shuang Zhang[1, 2‡]

[1]*School of Physics & Astronomy, University of Birmingham,*

Birmingham, B15 2TT, UK

[2] *Center for Terahertz Waves and College of Precision Instrument and Optoelectronics*

Engineering, Tianjin University and the Key Laboratory of Optoelectronics

Information and Technology (Ministry of Education), Tianjin 300072, China

[3]*College of Advanced Interdisciplinary Studies, National University of Defense*

Technology, Changsha 410073, China

[4]*Department of Physics, The Pennsylvania State University, University Park,*

Pennsylvania 16802-6300, USA

[5]*School of Electrical and Computer Engineering, Oklahoma State University, Stillwater,*

OK 74078, USA

**These authors contributed equally to this work*

[†]*Corresponding E-mail: jiaghan@tju.edu.cn*

[††]*Corresponding E-mail: cxl56@psu.edu*

[‡]*Corresponding E-mail: s.zhang@bham.ac.uk*

Abstract:

Nodal line semimetals exhibiting line degeneracies in the three-dimensional momentum space have been demonstrated recently. In general, the presence of nodal line semimetals is protected by special symmetries, such as mirror symmetry. However, these symmetries are usually necessary but not sufficient conditions as nodal lines can be annihilated even without breaking them. Very recently, nodal line semimetal possessing hourglass-shaped band structure emerges as a more robust candidate, where line degeneracies cannot be annihilated while preserving all underlying spatial symmetries. Here, for the first time, we experimentally demonstrate the presence of hourglass nodal line (HNL) in photonic meta-crystal at microwave frequency. We observe the HNL through near field scanning of the spatial fields followed by subsequent Fourier transformations. The observed photonic HNL resides in a clean and large frequency interval and is immune to symmetry preserving perturbation, which provides an ideal robust platform for photonic applications, such as anomalous quantum oscillation, spontaneous emission and resonant scattering.

Introduction

Topological physics has attracted great interests in the past decades [1-4], which usually requires for the protection by symmetries, such as time-reversal and mirror symmetries. Depending on whether there is a complete gap between valence and conduction bands, symmetry protected topological phases can be categorized into two classes, those that are gapped and gapless [3]. The gapped nontrivial topological phases

include topological insulators and superconductors [5]. Based on the dimension of degeneracies in the momentum space, the gapless topological phases can be sorted as Weyl/Dirac semimetals (0D), nodal line/chain semimetals (1D) and nodal surface semimetals (2D) [4]. The concepts of topological band theory and nontrivial topological phases have been extended from solid state systems into photonic systems in the last decade. Various topological phenomena have been realized in photonics, such as photonic quantum Hall effect [6-9], topological insulator [10-15], Weyl/Dirac semimetals [16-26] and nodal lines [27,28]. Among them, Weyl semimetals requiring breaking of either time-reversal or inversion symmetry are robust under general perturbations, as all three Pauli matrices have been involved exhaustively. Nodal line semimetals [27-36] with line degeneracies (1-D) only consist two of the anti-commuting Pauli matrices, hence extra symmetry constraints are required to make it stable. However, simple point symmetries only provide the orthogonality condition between different modes and cannot robustly guarantee the existence of nodal line. For example, most of nodal line semimetals arise from accidental degeneracy between two bands with opposite mirror eigenvalues, as shown in FIG. 1(a). Such nodal lines can be easily broken or removed from the Brillouin zone (BZ) by certain perturbations, such as structure variation, without breaking any underlying symmetries, as schematically shown in FIG. 1(c).

To overcome the fragileness of the typical nodal line semimetals, hourglass nodal line (HNL) [37,38] is proposed, which is formed by hourglass-shaped band dispersion

around a loop in the momentum space as shown in FIG. 1(b). The formation of HNL involves four bands, in contrast to only two bands in previous demonstration of nodal lines. FIG. 1(d) shows its robustness against symmetry preserving perturbations. Even when the double degeneracy points are flipped upside down $(1 \leftrightarrow 2)$, the hourglass-shaped zigzag pattern still persists. Thus, HNL provides a robust platform for future applications. Here, we theoretically propose the presence of HNL in a meta-crystal at microwave region, and for the first time, experimentally demonstrate HNL in photonics.

Results

Theoretical analysis of HNL in photonic meta-crystal

For the meta-crystal, each unit cell consists of two sets of structures α_1 and α_2, as shown in the left panel of FIG. 2(a), where each set includes two coupled metallic splitting resonant rings. The bottom/top view of the structure is shown in the right panel of FIG. 2(a). In the microwave regime, those metallic components are regarded as perfect electric conductor (PEC). The photonic meta-crystal is constructed in a simple tetragonal lattice (lattice periods are $p_x = p_y = 4mm$, $p_z = 5mm$) with metallic structures embedded in a hosting materials with dielectric constant of 2.2. The lattice possesses nonsymmorphic space group P4/nbm (No.125), which includes three glide mirror operations involving half lattice translation, $\tilde{M}_x : (x, y, z) \to \left(-x, y + \frac{1}{2}, z\right)$, $\tilde{M}_y : (x, y, z) \to \left(x + \frac{1}{2}, -y, z\right)$ and

$\tilde{M}_z:(x,y,z)\to\left(x+\frac{1}{2},y+\frac{1}{2},-z\right)$. The tilde above the mirror operation symbol indicates that it is a nonsymmorphic symmetry operator. These are crucial in our analysis. FIG. 2(b) shows the tetragonal BZ and surface BZ with the reduced BZ boxed by red lines and high symmetry points highlighted by red spheres. In this paper, the theoretical results are calculated by 'Eigenmode Solver' module of CST Microwave Studio [39].

The photonic HNL is located on the $k_z=\pi/p_z$ plane (Z-A-Y plane) highlighted in yellow in FIG. 2(b). The bands located on the BZ boundaries of $k_z=\pi/p_z$ plane (e.g. the line $\mathrm{X}-\mathrm{A}-\mathrm{Y}$) are all doubly degenerate due to the anti-commutation relation between $\tilde{M}_z$ and $\tilde{M}_y$ (or $\tilde{M}_x$). Consider an arbitrary point P located on A-Y line as an example, the combination of $\tilde{M}_z$ and $\tilde{M}_y$ yields,

$$\begin{aligned}\tilde{M}_z\tilde{M}_y:(x,y,z)&\to\left(x+1,-y+\frac{1}{2},-z\right)\\ \tilde{M}_y\tilde{M}_z:(x,y,z)&\to\left(x+1,-y-\frac{1}{2},-z\right)\end{aligned}\tag{1}$$

Let $|\varphi\rangle$ be an arbitrary common eigenstate of $\tilde{M}_z$ operator and the Hamiltonian at P point. We have $\tilde{M}_y\tilde{M}_z|\varphi\rangle=e^{ik_xp_x}e^{ik_yp_y/2}C_{2x}|\varphi\rangle$ and $\tilde{M}_z\tilde{M}_y|\varphi\rangle=e^{-ik_yp_y}\left(e^{ik_xp_x}e^{ik_yp_y/2}C_{2x}|\varphi\rangle\right)$, where C_{2x} is two-fold rotation about the *x*-axis. Since $k_y=\pi/p_y$ at P point, we obtain $\tilde{M}_z\tilde{M}_y|\varphi\rangle=-\tilde{M}_y\tilde{M}_z|\varphi\rangle$. Thus, we obtain the anti-commutation relation [40] between $\tilde{M}_z$ and $\tilde{M}_y$,

$$\left\{\tilde{M}_y,\tilde{M}_z\right\}=0\tag{2}$$

As $|\varphi\rangle$ is an eigenstate of $\tilde{M}_z$, we have $\tilde{M}_z|\varphi\rangle=\xi|\varphi\rangle$, where $\xi=1$ (or -1) is

eigenvalue of $\tilde{M}_z$. Then $\tilde{M}_z\tilde{M}_y|\varphi\rangle = -\xi\tilde{M}_y|\varphi\rangle$. Due to the anti-commutation in Eq.2, one obtains,

$$\langle\varphi|\tilde{M}_y|\varphi\rangle = \langle\varphi|\tilde{M}_z^{-1}\tilde{M}_z\tilde{M}_y|\varphi\rangle = -\langle\varphi|\tilde{M}_y|\varphi\rangle \quad (3)$$

ensuring the orthogonality between $|\varphi\rangle$ and $\tilde{M}_y|\varphi\rangle$. Both the states $|\varphi\rangle$ and $\tilde{M}_y|\varphi\rangle$ are eigenstates of the Hamiltonian, and due to opposite eigenvalues of operator $\tilde{M}_z$, they are degenerate, leading to the conclusion that all the eigenstates are doubly degenerate at any arbitrary point on A-Y line.

Next, we show that the double degeneracy at Z point is protected by higher irreducible representations of D_{4h}. As we know each unit cell contains two sets α_1 and α_2. Each set includes two perpendicularly positioned splitting resonant rings. For the wave propagating along *z* direction at low frequency, there exist a pair of hybrid modes arising from the in-phase and out-phase coupling between α_1 and α_2. In addition, due to the C_4 symmetry ($\frac{\pi}{2}$ rotation about *z* axis) of the crystal, there exists another pair of in-phase/out-phase coupled hybrid modes, which is related to the former pair of modes by a C_4 rotation. Therefore, there must exist a pair of degenerate modes due to the in-phase coupling between the two set α_1 and α_2, and another pair of degenerate modes originating from the out-phase coupling [39]. More mathematically, the little group (or wavevector group) at Z point is D_{4h} (or $4/\mathrm{mmm}$ in Hermann-Mauguin notation). The two pairs of degenerate frequencies due to the in-phase and out-phase coupling belong to higher irreducible representations E_u and E_g, which possess $\tilde{M}_z$ eigenvalue 1 and -1, respectively.

Finally, hourglass shaped band dispersion will be formed as the four bands travel from Z point to an arbitrary point P on A-Y line. $\tilde{M}_z$ symmetry exists for the whole $k_z = \pi / p_z$ plane, and thus any states on this plane can be labeled by the eigenvalue of $\tilde{M}_z$ (blue or red lines in FIG. 1b, d and FIG. 2c). Since the two degenerate bands possess the same eigenvalue of $\tilde{M}_z$ at Z point and opposite eigenvalues at point P, there must exist a pair-switching along Z-P line, and the two crossing bands must possess opposite eigenvalues, thus leading to hourglass shaped band dispersion, as shown in FIG. 2(c). As P point can freely move along the BZ boundaries on the $k_z = \pi / p_z$ plane (e.g. X-A-Y line), an hourglass ring naturally shows up, which ensures the appearance of HNL. A quarter view of the HNL is given in FIG. 2(d). The nodal degeneracy is highlighted by the red lines. The band structure along the high symmetry lines is plotted in FIG. 2(e), from which one can see a nearly ideal photonic HNL located in a quite broad and clean frequency range with the frequency variation ($\Delta\omega / \omega_{middle}$) less than 1%.

Experimental observation of photonic HNL

The sample is fabricated by the standard printed circuit board (PCB) technique. FIG. 3(a) shows the top view of the structure layer with thickness of 2mm. In addition, a 3-mm-thick spacer layer, made of dielectric material (F4BM) with the relative permittivity of 2.2, is placed between the adjacent copper-clad PCBs to prevent short contacting from metallic wires. Each layer of the PCB sample has 100×100 unit cells. By stacking the PCB sample layer by layer along z direction (9 unit cells), we

construct a photonic meta-crystal in the microwave band. Near-field scanning is carried out to map the HNL bulk band dispersion. In our experimental configuration, one *z*-oriented electrical dipole antenna acting as source is positioned at the side of the sample (as shown in FIG.3b). Another *z*-oriented electrical dipole antenna serving as probe raster-scans the top surface of the sample. The distance between the probe antenna and the top surface is around 1 mm, ensuring the sensitive detection of evanescent tails of the bulk states. Both the source and probe electrical dipoles are connected to a vector network analyzer (VNA: Keysight-N5234B, 10MHz-43.5GHz), which can measure both the amplitude and phase of electromagnetic field simultaneously in a broad frequency range. FIG. 3(b) gives the experiment set-up with source and probe denoted by red and blue cylinders, respectively. Its top surface illustrates real part of E_z at frequency of 14.8GHz. By performing subsequent Fourier transformation upon the detected spatial fields, we obtain the projected equi-frequency contours (EFCs) containing a series of discretized k_z values on the surface BZ. The torus in FIG. 3(c) shows the theoretical bulk EFC at 14.8GHz. Four lines $k_x = k_y \tan\theta$, $k_y = 0.2\pi/p_y$, $k_y = 0.4\pi/p_y$ and $k_y = 0.8\pi/p_y$ on the surface BZ are denoted by D, E, F and G, respectively. They correspond to four cases in FIG. 3(d), (e), (f) and (g). The left and right panels in FIG. 3(d) show the experimentally measured and theoretical simulated band spectrum along the line $k_x = k_y \tan\frac{\pi}{6}$ in the surface BZ, respectively. The white (left panel) and red (right panel) lines denote the light cone. Although the modes from crystals inside the light cone cannot be easily distinguished due to mixed projected bulk bands in air medium, the hourglass shaped

bands denoted by the white dashed lines located outside the light cone can be clearly recognized. The red dashed line in the theoretical panel denotes the hourglass shaped bulk bands on $k_z = \pi / p_z$ plane. Clearly, density of states vanishes around the hourglass node. Similarly, the left and right panels in FIG. 3(e), (f) and (g) illustrate the experimentally measured and theoretical simulated band spectra along the lines of $k_y = 0.2\pi / p_y$, $0.4\pi / p_y$ and $0.8\pi / p_y$, respectively. The $k_y = 0.2\pi / p_y$ and $0.4\pi / p_y$ lines in the surface BZ intersect with HNL, showing linear crossings in their dispersions. On the other hand, the $k_y = 0.8\pi / p_y$ line is located outside the HNL, exhibiting a band gap in the spectrum.

The experimentally measured EFCs in momentum space at 14.8GHz, 15.16GHz and 15.65GHz, which correspond to frequencies below, approaching and above experimental HNL, are shown in FIG. 4(a), (b) and (c), respectively. The positions of the second band (b2) and third band (b3) are indicated by white arrows, where b2 and b3 are two relevant bands forming HNL as shown in FIG. 2(c). The circle in the center denoted by the white line indicates the light cone. The two EFCs at 14.8GHz located far away from the light cone are easily distinguished. At frequency of 15.16GHz, the two EFCs nearly merge into each other. The third band at frequency of 15.65GHz is very close to the light cone, which makes it hard to distinguish. The theoretical simulated EFCs at the frequency of 14.2GHz, 14.45GHz and 14.75GHz, which correspond to frequencies below, approaching and above theoretical HNL, are illustrated in FIG. 4(d), (e) and (f), respectively. Comparing with the experimental

results in FIG.3 and FIG.4, the theoretical results show strong resemblance with the experimental ones except for small frequency shift due to fabrication inaccuracy.

To summarize, we theoretically propose HNL in a carefully designed photonic meta-crystal, which is protected by glide mirror symmetry and high irreducible representation of D_{4h}. The glide mirror involving fractional lattice translation causes the anti-commutation relation (Eq. 2) and then result in double degeneracy at BZ edge, that is crucial to the realization of HNL. By performing near-field scanning in the microwave region, for the first time, we experimentally observed the HNL in photonic meta-crystal structure, which provides a powerful platform for studying topological phases. Also, the HNL can support negative refraction [41], which usually requires simultaneously well-designed negative effective permittivity and permeability in overlapped frequency range. Other photonic applications that arise from the unique density of states of the nodal line include black-body radiation [42], spontaneous emission and resonant scattering [43]. With introduction of pseudo-magnetic field (synthetic vector potential), anomalous quantum oscillation may also be observed in the HNL [44].

Acknowledgements

We acknowledge the support from ERC Consolidator Grant (TOPOLOGICAL), Horizon 2020 Action (Project No. 734578), National Natural Science Foundation of China (grant 11604216) and the Chinese Scholarship Council Grant No. 201606250059, (LX). C.X. L. acknowledges the support from Office of Naval Research (Grant No. N00014-15-1-2675).

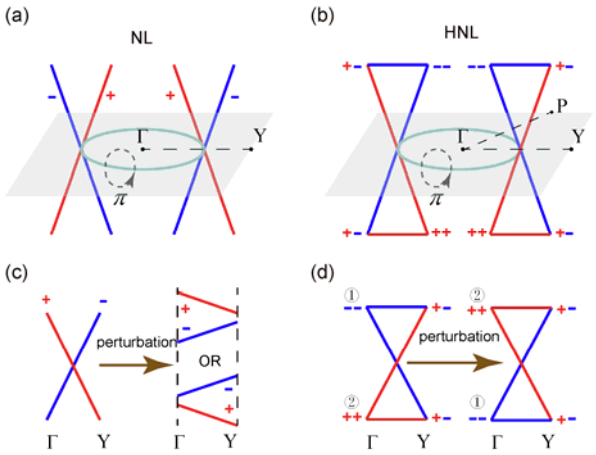

FIG. 1 (a) Nodal lines formed by accidental degeneracy possess opposite eigenvalues of mirror symmetry. (b) HNL formed by hourglass shaped band dispersion going around Γ point a circle. (c) Schematically illustrating that nodal line degeneracy is removed by perturbations. (d) Schematically illustrating the robustness of HNL. Note: The blue and red bands correspond to negative (-1) and positive $(+1)$ eigenvalue of the mirror symmetries. Γ and Y denote the BZ center and edge points, respectively.

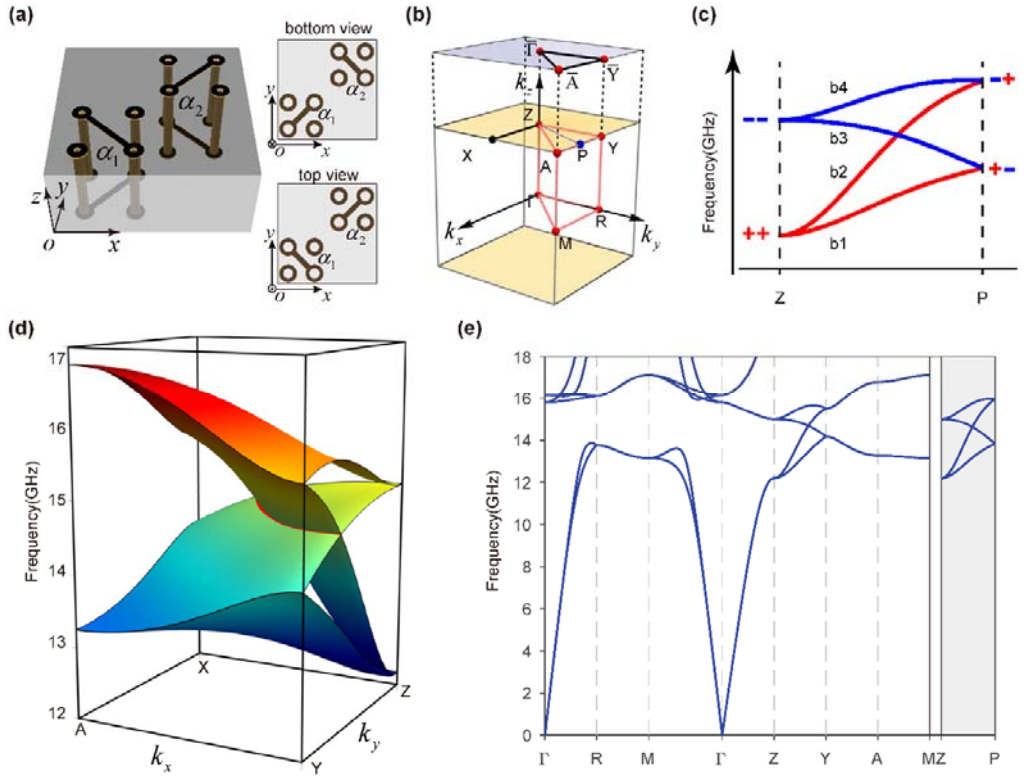

FIG. 2 (a) Unit cell of metallic structure layer with in-pane period $p_x = p_y = 4mm$ and thickness of $2mm$ are shown in the left panel. Between two structure layers, there is a spacer layer with thickness of 3mm. The bottom/top view of the metallic layer is given in the right panel. (b)The first (bulk) BZ of tetragonal lattice with reduced (bulk) BZ boxed by red triangle prism. The $k_z = \pi / p_z$ plane is highlighted in yellow, where HNL exists. The upper blue plane shows the surface BZ. (c) The hourglass shaped dispersion along line Z-P as indicated in (b). The red and blue lines are bands corresponding to glide mirror ($\tilde{M}_z$) eigenvalue of +1 and -1, respectively. b1, b2, b3 and b4 are four bands forming hourglass shaped dispersion. (d) The quarter view of photonic HNL dispersion on $k_z = \pi / p_z$ plane. The HNL degeneracy is plotted in red. (e) The bulk bands dispersion along high symmetry lines.

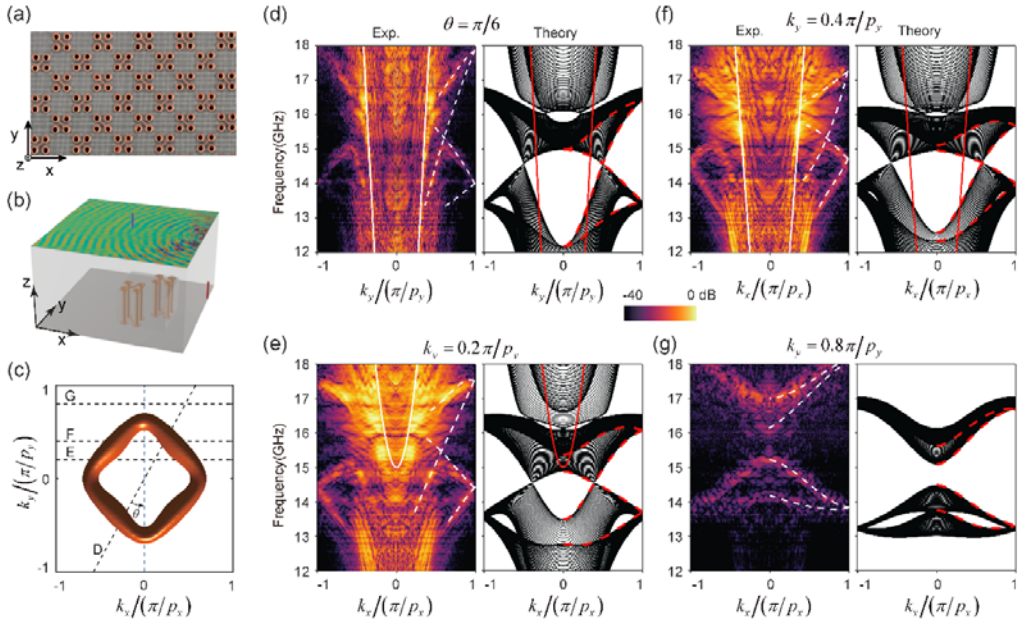

FIG. 3 (a) Photograph of top surface of the sample fabricated by printed circuit board technology. (b) Experiment set up configuration with source denoted by red cylinder and probe denoted by blue cylinder, respectively. The top surface illustrates the real part of electric field E_z at frequency of 14.8GHz. The structure unit cell is shown in the inset. (c) The theoretical equi-frequency contour at 14.8GHz near the HNL, which is shaped in torus. The four dashed lines $k_x = k_y \tan\theta$, $k_y = 0.2\pi/p_y$, $k_y = 0.4\pi/p_y$ and $k_y = 0.8\pi/p_y$ labelled by D, E, F and G in the surface BZ correspond to four cases (d), (e), (f) and (g), respectively. (d) The experiment (left panel) and theoretical (right panel) band projection when $\theta = \pi/6$. (e-g) The experiment (left panel) and theoretical (right panel) band projection along $k_y = 0.2\pi/p_y$, $0.4\pi/p_y$ and $0.8\pi/p_y$ line, respectively. The two lines $k_y = 0.2\pi/p_y$ and $0.4\pi/p_y$ intersect with the HNL. The $k_y = 0.8\pi/p_y$ line locates outside the HNL. Note that in FIG.3 (d-g), the white line (left panel) and red line (right panel) denote light cone. The white dashed lines in

the left panel illustrate hourglass shaped band dispersion. In the right panel, the red dashed lines show hourglass shaped band dispersion simulated on $k_z = \pi / p_z$.

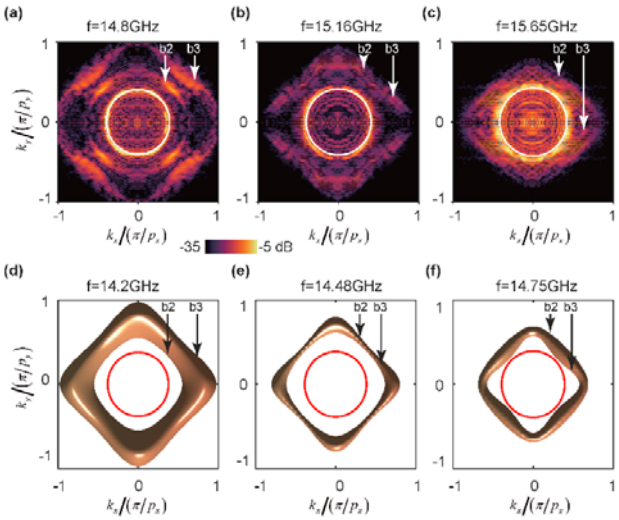

FIG. 4 (a-c) The experimental results of projected E_z field at frequency of 14.8GHz, 15.16GHz and 15.65GHz, respectively. The positions of the second band (b2) and third band (b3) are pointed out by white arrows, where b2 and b3 are hourglass shaped bands as denoted in FIG. 2(c). The white circles denote the light cone. (d-f) The theoretical results of EFCs at frequency of 14.2GHz, 14.48GHz and 14.75GHz, respectively. The red circles denote the light cone.

References:

[1] M. Z. Hasan and C. L. Kane, Reviews of Modern Physics **82**, 3045 (2010).

[2] X.-L. Qi and S.-C. Zhang, Reviews of Modern Physics **83**, 1057 (2011).

[3] C.-K. Chiu, J. C. Y. Teo, A. P. Schnyder, and S. Ryu, Reviews of Modern Physics **88**, 035005 (2016).

[4] N. P. Armitage, E. J. Mele, and A. Vishwanath, Reviews of Modern Physics **90** (2018).

[5] A. P. Schnyder, S. Ryu, A. Furusaki, and A. W. W. Ludwig, Physical Review B **78** (2008).

[6] F. D. Haldane and S. Raghu, Phys Rev Lett **100**, 013904 (2008).

[7] Z. Wang, Y. Chong, J. D. Joannopoulos, and M. Soljačić, Nature **461**, 772 (2009).

[8] Y. Poo, R.-x. Wu, Z. Lin, Y. Yang, and C. T. Chan, Physical Review Letters **106** (2011).

[9] K. Fang, Z. Yu, and S. Fan, Nature Photonics **6**, 782 (2012).

[10] A. B. Khanikaev, S. Hossein Mousavi, W.-K. Tse, M. Kargarian, A. H. MacDonald, and G. Shvets, Nature Materials **12**, 233 (2012).

[11] M. C. Rechtsman, J. M. Zeuner, Y. Plotnik, Y. Lumer, D. Podolsky, F. Dreisow, S. Nolte, M. Segev, and A. Szameit, Nature **496**, 196 (2013).

[12] W.-J. Chen, S.-J. Jiang, X.-D. Chen, B. Zhu, L. Zhou, J.-W. Dong, and C. T. Chan, Nature Communications **5**, 5782 (2014).

[13] L.-H. Wu and X. Hu, Physical Review Letters **114**, 223901 (2015).

[14] A. Slobozhanyuk, S. H. Mousavi, X. Ni, D. Smirnova, Y. S. Kivshar, and A. B. Khanikaev, Nature Photonics **11**, 130 (2016).

[15] Y. Yang, Z. Gao, H. Xue, L. Zhang, M. He, Z. Yang, R. Singh, Y. Chong, B. Zhang, and H. Chen, arXiv:1804.03595 (2018).

[16] L. Lu, L. Fu, J. D. Joannopoulos, and M. Soljačić, Nature Photonics **7**, 294 (2013).

[17] L. Lu, Z. Wang, D. Ye, L. Ran, L. Fu, J. D. Joannopoulos, and M. Soljačić, Science **349**, 622 (2015).

[18] W.-J. Chen, M. Xiao, and C. T. Chan, Nature Communications **7**, 13038 (2016).

[19] M. Xiao, Q. Lin, and S. Fan, Physical Review Letters **117**, 057401 (2016).

[20] Q. Lin, M. Xiao, L. Yuan, and S. Fan, Nature Communications **7**, 13731 (2016).

[21] W. Gao, B. Yang, M. Lawrence, F. Fang, B. Béri, and S. Zhang, Nature Communications **7**, 12435 (2016).

[22] J. Noh, S. Huang, D. Leykam, Y. D. Chong, K. P. Chen, and Mikael C. Rechtsman, Nature Physics **13**, 611 (2017).

[23] Q. Guo, B. Yang, L. Xia, W. Gao, H. Liu, J. Chen, Y. Xiang, and S. Zhang, Physical Review Letters **119**, 213901 (2017).

[24] Q. Wang, M. Xiao, H. Liu, S. Zhu, and C. T. Chan, Physical Review X **7**, 031032 (2017).

[25] L. Xia, W. Gao, B. Yang, Q. Guo, H. Liu, J. Han, W. Zhang, and S. Zhang, Laser & Photonics Reviews **12**, 1700226 (2017).

[26] B. Yang, Q. Guo, B. Tremain, R. Liu, L. E. Barr, Q. Yan, W. Gao, H. Liu, Y. Xiang, J. Chen, C. Fang, A. Hibbins, L. Lu, and S. Zhang, Science (2018).

[27] Q. Yan, R. Liu, Z. Yan, B. Liu, H. Chen, Z. Wang, and L. Lu, Nature Physics **14**, 461 (2018).

[28] W. Gao, B. Yang, B. Tremain, H. Liu, Q. Guo, L. Xia, A. P. Hibbins, and S. Zhang, Nature Communications **9**, 950 (2018).

[29] Y. Kim, B. J. Wieder, C. L. Kane, and A. M. Rappe, Physical Review Letters **115**, 036806 (2015).

[30] F. Chen, W. Hongming, D. Xi, and F. Zhong, Chinese Physics B **25**, 117106 (2016).

[31] T. Bzdušek, Q. Wu, A. Rüegg, M. Sigrist, and A. A. Soluyanov, Nature **538**, 75 (2016).

[32] G. Bian, T.-R. Chang, R. Sankar, S.-Y. Xu, H. Zheng, T. Neupert, C.-K. Chiu, S.-M. Huang, G. Chang, I. Belopolski, D. S. Sanchez, M. Neupane, N. Alidoust, C. Liu, B. Wang, C.-C. Lee, H.-T. Jeng, C. Zhang, Z. Yuan, S. Jia, A. Bansil, F. Chou, H. Lin, and M. Z. Hasan, Nature Communications **7**, 10556 (2016).

[33] J. He, X. Kong, W. Wang, and S.-P. Kou, arXiv:1709.08287 (2017).

[34] M. Hirayama, R. Okugawa, T. Miyake, and S. Murakami, Nature Communications **8**, 14022 (2017).

[35] T. Kawakami and X. Hu, Physical Review B **96**, 235307 (2017).

[36] R. Okugawa and S. Murakami, Physical Review B **96**, 115201 (2017).

[37] R. Takahashi, M. Hirayama, and S. Murakami, Physical Review B **96**, 155206 (2017).

[38] B. Fu, X. Fan, D. Ma, C.-C. Liu, and Y. Yao, Physical Review B **98**, 075146 (2018).

[39] See details in supplementary information.

[40] X.-Y. Dong and C.-X. Liu, Physical Review B **93**, 045429 (2016).

[41] L. Wang, S.-K. Jian, and H. Yao, Physical Review A **93**, 061801 (2016).

[42] P. J. Roberts, in *IEE Colloquium on Semiconductor Optical Microcavity Devices and Photonic Bandgaps (Digest No. 1996/267)*1996), pp. 4/1.

[43] M. Zhou, L. Ying, L. Lu, L. Shi, J. Zi, and Z. Yu, Nature Communications **8**, 1388 (2017).

[44] H. Yang, R. Moessner, and L.-K. Lim, Physical Review B **97**, 165118 (2018).